International Journal of Pharmaceutics 390 (2010) 234–241

Contents lists available at ScienceDirect

International Journal of Pharmaceutics

journal homepage: www.elsevier.com/locate/ijpharm

Pharmaceutical Nanotechnology

Transferrin-conjugated lipid-coated PLGA nanoparticles for targeted delivery of aromatase inhibitor 7α-APTADD to breast cancer cells

Yu Zheng[a,b], Bo Yu[d,e], Wanlop Weecharangsan[a], Longzhu Piao[a], Michael Darby[c], Yicheng Mao[a,e], Rumiana Koynova[a], Xiaojuan Yang[a], Hong Li[a], Songlin Xu[a], L. James Lee[d,e], Yasuro Sugimoto[c], Robert W. Brueggemeier[c], Robert J. Lee[a,e,*]

[a] Division of Pharmaceutics, College of Pharmacy, the Ohio State University, Columbus, OH 43210, USA
[b] State Key Laboratory of Biotherapy, West China Hospital, the Sichuan University, Chengdu, Sichuan 610041, PR China
[c] Division of Medicinal Chemistry and Pharmacognosy, the Ohio State University, Columbus, OH 43210, USA
[d] Department of Chemical and Biomolecular Engineering, the Ohio State University, Columbus, OH 43210, USA
[e] NSF Nanoscale Science and Engineering Center (NSEC) for Affordable Nanoengineering of Polymeric Biomedical Devices (CANPBD), the Ohio State University, Columbus, OH 43210, USA

ARTICLE INFO

Article history:
Received 6 October 2009
Received in revised form 29 January 2010
Accepted 8 February 2010
Available online 13 February 2010

Keywords:
Aromatase inhibitor
PLGA nanoparticle
Transferrin receptor
7α-APTADD
Drug targeting

ABSTRACT

Transferrin (Tf)-conjugated lipid-coated poly(d,l-lactide-co-glycolide) (PLGA) nanoparticles carrying the aromatase inhibitor, 7α-(4′-amino)phenylthio-1,4-androstadiene-3,17-dione (7α-APTADD), were synthesized by a solvent injection method. Formulation parameters including PLGA-to-lipid, egg PC-to-TPGS, and drug-to-PLGA ratios and aqueous-to-organic phase ratio at the point of synthesis were optimized to obtain nanoparticles with desired sizes and drug loading efficiency. The optimal formulation had a drug loading efficiency of 36.3 ± 3.4%, mean diameter of 170.3 ± 7.6 nm and zeta potential of −18.9 ± 1.5 mV. The aromatase inhibition activity of the nanoparticles was evaluated in SKBR-3 breast cancer cells. IC_{50} value of the Tf-nanoparticles was ranging from 0.77 to 1.21 nM, and IC_{50} value of the nanoparticles was ranging from 1.90 to 3.41 nM ($n = 3$). The former is significantly lower than the latter ($p < 0.05$). These results suggested that the aromatase inhibition activity of the Tf-nanoparticles was enhanced relative to that of the non-targeted nanoparticles, which was attributable to Tf receptor (TfR) mediated uptake. In conclusion, Tf-conjugated lipid-coated PLGA nanoparticles are potential vehicles for improving the efficiency and specificity of therapeutic delivery of aromatase inhibitors.

1. Introduction

Aromatase is a part of the cytochrome P450 enzyme complex that catalyzes the conversion of androgen to estradiol, and its expression is elevated in breast cancer tissues relative to normal breast tissues (James et al., 1987; Reed et al., 1989; Bulun et al., 1993; Miller et al., 1997). Currently, aromatase inhibitors anastrozole, letrozole and exemestane are first line therapeutic agents for estrogen responsive breast cancer (Brueggemeier et al., 2005). 7α-APTADD is a potent irreversible aromatase inhibitor with high affinity to its target (Snider and Brueggemeier, 1987). Its activity has been shown in many cell lines including human mammary carcinoma MCF-7 cells and choriocarcinoma JAr cells (Brueggemeier and Katlic, 1990). In addition, therapeutic effect of this drug has been shown *in vivo* in a rat mammary carcinoma model (Brueggemeier et al., 1997).

7α-APTADD is insoluble in water, which may adversely affect its oral bioavailability and requires a solubilization vehicle for systemic delivery. Nanoparticles, including liposomes, can facilitate solubilization of hydrophobic drugs and increase drug accumulation in the tumor through the enhanced permeability and retention (EPR) effect (Minko, 2006). In addition, it is possible to target the delivery of nanoparticles to tumor cells via conjugation to a targeting ligand. Formulation of anticancer drugs such as doxorubicin into liposomes has been shown to enhance their therapeutic efficacy and reduce certain toxicities (Lu et al., 2007). However, according to our preliminary experiment, 7α-APTADD cannot be efficiently entrapped into liposomes. Therefore, a PLGA nanoparticle based strategy was developed in this study.

PLGA is a biodegradable and biocompatible polymer frequently used in drug delivery (Jain, 2000). PLGA nanoparticles can readily incorporate hydrophobic drugs (Budhian et al., 2007). PLGA, in nanosize, has a relatively rapid rate of hydrolysis (Duncanson et

* Corresponding author at: College of Pharmacy, 500 W. 12th Ave., Columbus, OH 43210, USA. Tel.: +1 614 292 4172; fax: +1 614 292 7766.
E-mail address: lee.1339@osu.edu (R.J. Lee).

0378-5173/$ – see front matter © 2010 Elsevier B.V. All rights reserved.
doi:10.1016/j.ijpharm.2010.02.008

al., 2007). It has been established in previous studies that coating of a PLGA core with amphiphilic lipids can possibly reduce access of the polymer to H_2O (Bershteyn et al., 2008; Chan et al., 2009), which in turn decreases the rate of PLGA hydrolysis and the associated drug release (Chan et al., 2009). Therefore, in this study, lipid-coated PLGA nanoparticles were investigated as drug carriers. In addition, Tf was conjugated to the nanoparticles. TfR is a dimeric transmembrane glycoprotein (180 kDa) (Yang et al., 2009) that is over-expressed in many types of tumor tissues (Shindelman et al., 1981; Faulk et al., 1980; Savellano et al., 2003; Rossiello et al., 1984). Besides, neoplastic cells with high metastatic potential have been shown to express higher levels of the TfR than those with low metastatic potential (Inoue et al., 1993). These make the TfR an attractive marker for tumor cell targeting. Tf, an 80 kDa glycoprotein, is the ligand for TfR (Yang et al., 2009), which is available in recombinant version (Novozymes, 2007) and, as a human protein, has low immunogenicity (Ali et al., 1999). In addition, Tf-conjugated nanoparticles have been shown to selectively deliver therapeutic agents including doxorubicin and cisplatin to tumor cells over-expressing TfR through TfR-mediated endocytosis (Eavarone et al., 2000; Iinuma et al., 2002). TfR-targeted drug delivery systems are potential candidates for clinical translation. In this study, Tf was conjugated to 7α-APTADD loaded nanoparticles to increase the efficiency and selectivity of delivery to breast cancer cells.

2. Materials and methods

2.1. Materials

7α-APTADD was synthesized as described previously (Snider and Brueggemeier, 1987). Egg phosphatidylcholine (egg PC) and 1,2-dioleoyl-sn-glycero-3-phosphoethanolamine (DOPE) were purchased from Avanti Polar Lipids (Alabaster, AL). D-α-tocopherol polyethylene glycol 1000 succinate (TPGS) was obtained as a gift from Eastman Co. Ltd. (Gwynedd, UK). Poly(d, l-lactide-co-glycolide), holo-human Tf, triethylamine, bovine serum albumin, sepharose CL-4B chromatography media, calcein, androst-4-ene-3,17-dione, bisbenzimide (Hoechst 33258), deoxyribonucleic acid (DNA), 3-maleimidobenzoic acid N-hydroxysuccinimide ester (MBS), phenazine methosulfate (PMS) and solvents were purchased from Sigma–Aldrich (St. Louis, MO, USA). DRAQ 5 was purchased from Biostatus Limited Inc. (Leicestershire, UK). SKBR-3 cells were obtained from American Type Culture Collection (ATCC) (Manassas, VA, USA). Fetal bovine serum was purchased from JHR Bioscience (Lenexa, KS, USA). Phenol red-free custom media (MEM, Earle's salts, 1.5× amino acids, 2× non-essential amino acids, L-glutamine, 1.5× vitamins), octadecyl-rhodamine B chloride (R18) and gentamicin were purchased from Invitrogen Corporation (Carlsbad, CA, USA). [1β-^{3}H(N)]-androst-4-ene-3,17-dione (specific activity 23.5 Ci/mmol) was purchase from PerkinElmer Inc. (Waltham, MA, USA). 3-(4,5-Dimethyl-thiazol-2yl)-5-(3-carboxymethoxyphenyl)-2-(4-sulfophenyl)-2H-tetrazolium (MTS) was purchased from Promega Corporation (Madison, WI, USA).

2.2. Preparation of 7α-APTADD loaded nanoparticles

PLGA, egg PC, TPGS and 7α-APTADD were co-dissolved in an acetone–ethanol solvent mixture (1:1, v/v). The solution was heated to 60 °C and rapidly injected into preheated deionized water at 60 °C using a 1 ml syringe with a 28 gauge needle. In this study, effects of four formulation parameters on particle size and drug loading efficiency were investigated, including: (1) PLGA-to-lipid ratio, (2) egg PC-to-TPGS ratio, (3) drug-to-PLGA ratio and (4) aqueous-to-organic phase ratio at the time of synthesis. Single factor test was used to optimize each parameter. The initial standard formulation used was: 13 mg egg PC, 2 mg TPGS, 15 μg of 7α-APTADD and 1 mg PLGA in 0.2 ml of acetone–ethanol mixture as the organic phase, and with 1 ml deionized water as the aqueous phase. All experiments were performed for three times.

2.3. Determination of loading efficiency

Drug loaded nanoparticles were separated from the free drug by size-exclusion chromatography on a Sepharose CL-4B column. To analyze drug concentration, 1.9 ml of acetonitrile was added into 0.1 ml of the nanoparticle suspension from the column fractions and vortexed for 2 min to dissolve all components of the nanoparticles. The 7α-APTADD content was then determined on an Agilent 1100 HPLC equipped with a Hypersil reverse phase C-18 column at 25 °C (250 mm × 4.6 mm, 5 μm; Thermo Scientific, MA, USA). 7α-APTADD absorbance was measured by an UV–vis detector at 243 nm and had a retention time of 6 min when eluted with 70:30 acetonitrile/water mobile phase at a flow rate of 1 ml/min. The loading efficiency of 7α-APTADD was calculated by dividing drug content in the nanoparticle fractions by the amount of drug added initially. All experiments were performed for three times.

2.4. Particle size and zeta potential

Three batches of nanoparticles were prepared using the optimal formulation. The nanoparticle size distribution was determined by dynamic light scattering on a model 370 Nicomp Submicron Particle Sizer (Particle Sizing Systems, Santa Barbara, CA) at room temperature. The zeta potential was determined on a ZetaPALS instrument at room temperature (Brookhaven Instruments Corp., Worcestershire, NY).

2.5. Preparation and characterization of 7α-APTADD loaded Tf-nanoparticles

A post-insertion method (Yang et al., 2009; Chiu et al., 2006) was adopted to incorporate Tf-DOPE ligand into the lipid bilayers of the 7α-APTADD loaded nanoparticles. First, maleimidobenzoyl-DOPE (MB-DOPE) was synthesized. MBS (15 μM, 4.7 mg) was dissolved in 1 ml chloroform and added to a 2 ml chloroform solution of DOPE (10 μM, 7.44 mg) containing 50 μl triethylamine. The solution was stirred overnight at room temperature, and then the solvent was evaporated and ethanol added to dissolve the product. The ethanol solution of MB-DOPE was rapidly injected into water and the MB-DOPE micelles were thus obtained. Meanwhile, Tf in HEPES buffer (pH 8) was activated with 5× Traut's reagent to yield Tf-SH. Then, the Tf-SH was mixed with micelles of MB-DOPE at a protein-to-lipid molar ratio of 1:10 and the mixture was incubated at 37 °C for 1 h. The resulting Tf-DOPE micelles were then incubated with 7α-APTADD loaded nanoparticle for 1 h at 37 °C to complete the post-insertion of Tf.

2.6. Cryogenic transmission electron microscopy (cryo-TEM)

7α-APTADD loaded nanoparticles and Tf-nanoparticles were prepared as described in Sections 2.2 and 2.3. Tf-liposomes were prepared as described in Sections 2.2 and 2.3 except without addition of PLGA. The morphology of the nanoparticles and the liposomes was examined by cryo-TEM. Samples for cryo-TEM were prepared as described previously (Yang et al., 2009). Briefly, a drop of the nanoparticles was applied on a perforated carbon film, supported by a copper grid and held by the controlled environment vitrification system. Then the grid was immediately plunged into liquid ethane at its melting point (−183 °C) and stored in liquid nitrogen (−196 °C). The vitrified sample was examined in a Tecnai G2 Transmission Electron Microscope (FEI Company, Oregon, USA)

operated at 120 kV using a Gatan HC3500 Tilt heating/Nitrogen cooling holder (Pleasanton, CA, USA). Digital images were captured by a Gatan 791 MultiScan CCD camera and processed using the Digital Micrograph 3.1 software package.

2.7. Colloidal stability of the nanoparticles

The colloidal stability of 7α-APTADD loaded nanoparticles and 7α-APTADD loaded Tf-nanoparticles was studied by monitoring the changes in the particle size during storage at 4 °C. At various time points, aliquots of each sample were withdrawn and the particle size distribution was determined by dynamic light scattering on a model 370 Nicomp Submicron Particle Sizer. Experiments were performed for three times.

2.8. Cell culture

A breast cancer cell line, SKBR-3, was maintained in phenol red-free custom media supplemented with glutamine (2 mM), 10% (v/v) fetal bovine serum and gentamicin (20 mg/l). Cells were cultured as a monolayer in a humidified atmosphere containing 5% CO_2 at 37 °C.

2.9. TfR expression on cell surface

TfR expression levels in breast cancer cells were measured by a fluorescein isothiocyanate (FITC) labeled Tf (FITC-Tf) binding assay, as described previously (Yang et al., 2009). For the study, 4×10^5 cells were incubated with 200 μg/ml FITC-Tf at 4 °C for 30 min. The cells were then washed twice with cold PBS (pH 7.4) containing 0.1% BSA, pelleted by centrifugation at 1500 RPM for 3 min and then resuspended in PBS. Cells without treatment were used as a negative control. Cellular fluorescence was measured by a FACSCalibur flow cytometer (Becton Dickinson, Franklin Lakes, NJ). Experiments were carried out in triplicate.

2.10. Cellular uptake of calcein loaded nanoparticles by flow cytometry

Calcein is a water soluble fluorescent dye with an excitation and emission wavelengths of 495 and 515 nm, respectively. Under a 488 nm excitation that is used by flow cytometry, calcein emits a strong signal in the typical cytometric FL1 channel (525 nm). Calcein loaded nanoparticles were prepared using the optimal formulation as described above except that the drug was not added into the organic phase. In addition, the organic phase was injected into preheated calcein aqueous solution (50 mM, pH 8). Then, free calcein was removed by passing the sample through a Sepharose CL-4B column. Calcein loaded Tf-nanoparticles were prepared by post-insertion, as described in Section 2.5, at Tf-DOPE-to-total lipid ratios of 0.3:100, 0.6:100, 1.5:100 and 3:100.

For cellular uptake studies, 4×10^5 cells were incubated at 37 °C in 1 ml complete culture media with or without 20 μM Tf (at a lipid concentration 72 μg/ml) for 2 h. Then, the cells were washed three times with PBS and fixed in 1% para-formaldehyde solution. Nanoparticle uptake in cells was analyzed by flow cytometry. Experiments were carried out in triplicate.

2.11. Cellular uptake of R18 labeled nanoparticles by confocal laser scanning microscopy

Octadecyl-rhodamine B chloride (R18), a lipophilic dye, was used to track the nanoparticles, as described previously (Chiu et al., 2006). R18 labeled nanoparticles were prepared using the optimal formulation by replacing 7α-APTADD with R18. Molar ratio of R18 to lipids used was 0.05:100. R18 labeled Tf-nanoparticles with 0.6 mol% of Tf-DOPE were prepared as described in Section 2.5.

For cellular uptake experiments, 4×10^5 cells were incubated at 37 °C in 1 ml complete culture media with or without 20 μM Tf (at a lipid concentration 72 μg/ml) for 2 h. Then, the cells were washed three times with PBS and fixed in 1% para-formaldehyde solution. The cells were stained by DRAQ 5 (a nuclear counterstain) and examined on a Zeiss LSM 510 META laser scanning confocal microscope (Zeiss, Oberkochen, Germany).

2.12. Cytoxicity assay for free drug and Tf-nanoparticles

The cytotoxicity of the free drug and the drug loaded nanoparticles was evaluated by MTS assay. 7α-APTADD loaded Tf-nanoparticles were prepared as described in Sections 2.2 and 2.3. Empty nanoparticles were prepared similarly except without addition of the drug. The SKBR-3 cells were seeded in 96-well plates at a density of 2×10^3 cells/well. After 24 h of incubation, the medium was replaced with fresh medium containing varying concentrations of 7α-APTADD dissolved in DMSO or 7α-APTADD loaded Tf-nanoparticles prepared by serial dilution. Empty nanoparticles of matching lipid concentration were diluted similarly. Cells without treatment or cultured in the same media containing either DMSO or empty nanoparticles were used as controls. Experiments were carried out in quadruplicate. After 24 h, the medium was aspirated. Twenty μl reagent composed of MTS and PMS at a volume ratio of 20:1 was added to each well containing 100 μl fresh media. After 1.5 h incubation at 37 °C, absorbance at 490 nm for formazan product of MTS conversion was detected on a Spectra MAX 340 plate reader (Molecular Devices Corp., Sunnyvale, CA, USA). The relative cell viability was calculated by dividing the absorbance in the samples treated with the test agents by the absorbance in the control samples.

2.13. Inhibition of aromatase in SKBR-3 cells

Drug loaded nanoparticles were prepared using the optimal formulation as described in Section 2.1. For the study, 1×10^5 SKBR-3 cells were seeded in 6-well plates. After 24 h of incubation, the medium was replaced with fresh medium containing varying concentrations of 7α-APTADD, 7α-APTADD loaded nanoparticles and 7α-APTADD loaded Tf-nanoparticles. Experiments were carried out in triplicate. After 2 h, the media with the test agents were removed and cells were washed with PBS. Then, 1 ml fresh medium containing [1β-^{3}H] androstenedione (8.2 pmol, 0.17 αCi) and androstenedione (193 pmol), as the substrates for aromatase, was added to each well. Cells cultured in the same media containing DMSO or empty nanoparticles were used as controls. After 3 h, the media were transferred into centrifuge tubes. The remaining substrate [1β-^{3}H] androstenedione in the media was extracted by 3 ml diethyl ether for 2 times, and the aqueous media was then treated by addition of 3% dextran-coated charcoal suspension (200 μl). After centrifugation, aliquot (0.6 ml) of the media was then added to complete scintillation cocktail (5.0 ml) and the [^{3}H] concentration was quantitatively determined by liquid scintillation counting. A modified Hoechst dye assay method was conducted to analyze DNA content (Rago et al., 1990). A NaOH (8 mM) solution (980 μl) was added to each well to lyse cells at 60 °C for 5 min and then a HEPES solution (1 M, 20 μl) was added to neutralize NaOH. Cell lysate (100 μl) was placed into each well of a 96-well plate and the Hoechst dye (20 μg/ml) was added to each well on the plate. The relative fluorescence units (RFU) were determined by a Tecan GENios reader (Tecan Systems, Inc., CA, USA). The excitation and emission wavelengths used were 360 and 465 nm, respectively. DNA in each sample was quantified using a standard curve of calfthymus DNA determined using the same method. The aro-

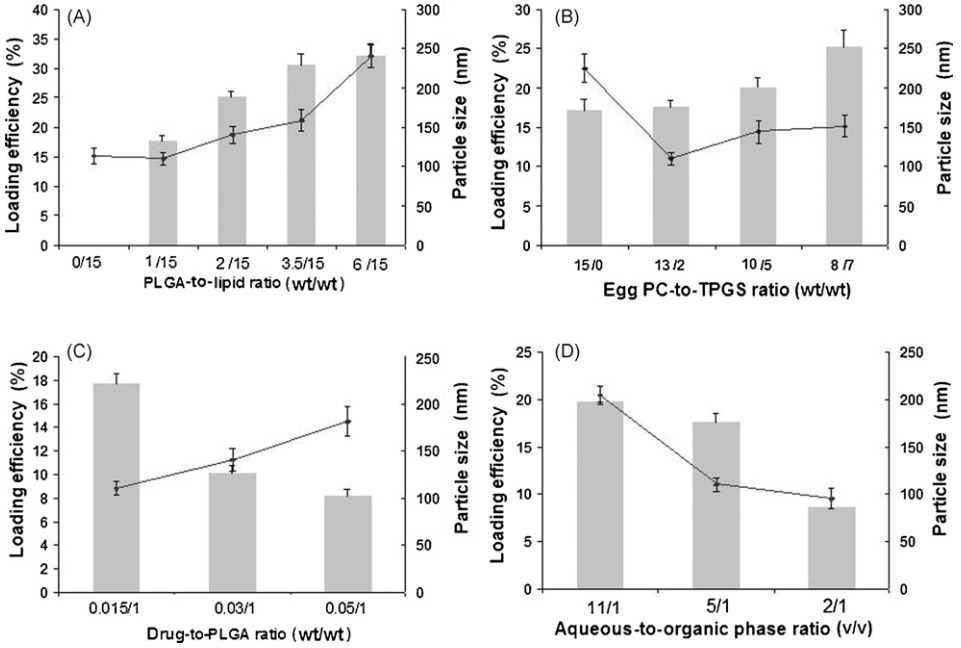

Fig. 1. Effects of four preparation variables on the particle size (♦) and loading efficiency ( ) of the 7α-APTADD loaded nanoparticle. PLGA-to-lipid (wt/wt) (A), egg PC-to-TPGS ratio (wt/wt) (B), drug-to-PLGA ratio (wt/wt) (C) and aqueous-to-organic phase ratio at the point of synthesis (v/v) (D) ($n = 3$).

matase activity was calculated by dividing the amount of [^{3}H] H_2O formed per hour to the DNA content. The relative aromatase inhibition activity was calculated by dividing the aromatase activity of the samples treated with the test agents by the aromatase activity of the control samples. Data was analyzed and plotted using GraphPad. Statistical differences were analyzed using one-way ANOVA.

3. Results and discussion

3.1. Preparation of 7α-APTADD loaded nanoparticles

Effects of composition and synthetic method on the size and the loading efficiency of the 7α-APTADD nanoparticles were investigated. The results are shown in Fig. 1. Particle size increased with the increase in PLGA-to-lipid ratio at PLGA-to-lipid ratios of ≥1/15 (Fig. 1A). This is possible because, as the PLGA-to-lipid ratio increased, the lipids in the formulation were insufficient to fully emulsify PLGA cores. It is important to note that the drug was not efficiently incorporated into the nanoparticles without PLGA in the formulation. These results suggested that addition of PLGA in the formulation was the key to stable drug loading. Besides, the loading efficiency increased with the PLGA-to-lipid ratio ($p < 0.05$), suggesting a high affinity between PLGA and the hydrophobic drug. The egg PC-to-TPGS ratio also influenced both the particle size and the loading efficiency (Fig. 1B). The particle size of the nanoparticles firstly decreased along with egg PC-to-TPGS ratio, then increased. TPGS has a poly(ethylene glycol) chain. The presence of poly(ethylene glycol) on the nanoparticle surface likely prevented the aggregation of the nanoparticles and decreased particle size (Chan et al., 2009). The subsequent increase in particle size at higher TPGS levels is relatively minor and not significant ($p > 0.05$). Meanwhile, drug loading efficiency slightly increased when the egg PC-to-TPGS ratio was at ≤ 3/2, and increased more rapidly thereafter ($p < 0.05$), which was also because TPGS provided steric stabilization of nanoparticles due to the hydrophilic PEG chain. The increase in the drug-to-PLGA ratio led to an apparent reduction in the loading efficiency ($p < 0.05$) and a significant increase in the particle size ($p < 0.05$) (Fig. 1C). Increase of the particle size with increase of the drug-to-PLGA ratio for the ethanol injection method has been reported earlier (Stano et al., 2004). By increasing the drug-to-PLGA ratio, more drugs

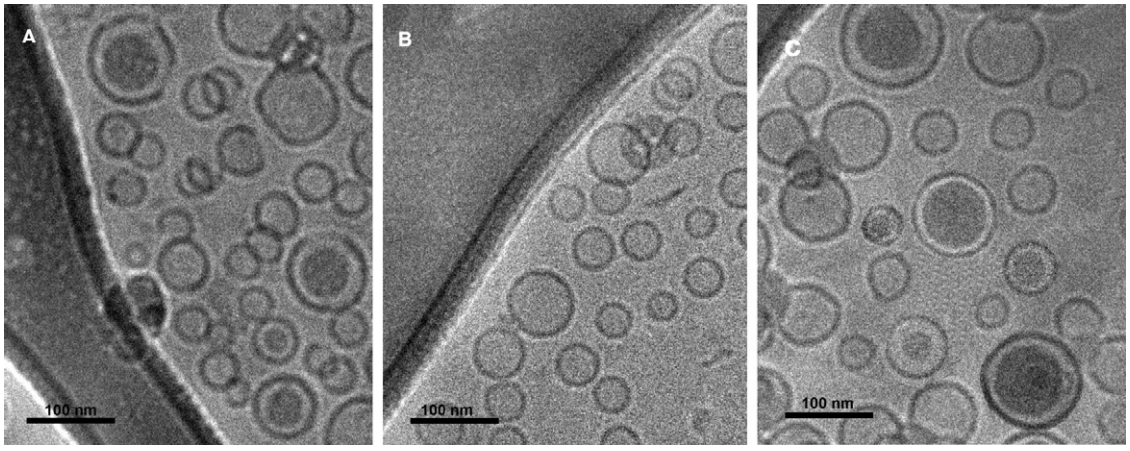

Fig. 2. The cryo-TEM images of the 7α-APTADD loaded Tf-nanoparticles (A), liposomes (B) and nanoparticles (C).

could be loaded into the nanoparticles. However, the increase of the entrapped drug was non-linear with respect to the increase of initially added drug, resulting in a decrease in the loading efficiency. During synthesis of the nanoparticles, the particle size and the loading efficiency decreased with decreasing of the aqueous-to-organic phase ratio ($p < 0.05$) (Fig. 1D). Based on these findings, an egg PC-to-TPGS ratio of 8/7, a drug-to-PLGA ratio of 0.015/1 and a PLGA-to-lipid ratio of 3.5/15 were identified as parameters for the optimal formulation.

The drug loading efficiency of this optimal formulation was $36.3 \pm 3.4\%$; the particle size was 170.3 ± 7.6 nm and the zeta potential was -18.9 ± 1.5 mV. Further, 7α-APTADD loaded Tf-nanoparticle with a Tf-DOPE content of 0.6 mol% was prepared using this formulation. The particle size was 187.0 ± 7.1 nm and the zeta potential was -17.3 ± 1.4 mV. Therefore, after insertion of Tf, the particle size was slightly increased whereas the zeta potential was not noticeably altered.

3.2. Cryo-TEM

Cryo-TEM images showed that both 7α-APTADD loaded nanoparticles, Tf-nanoparticles and Tf-liposomes were spherical in shape. The 7α-APTADD loaded nanoparticles and the Tf-nanoparticles exhibited two coexisting nanostructures: liposomes and nanoparticles with a core–shell structure (Fig. 2). The core–shell structure was possibly composed of a hydrophobic PLGA core and a shell formed by a phospholipid bilayer. No significant differences were observed between images of 7α-APTADD loaded Tf-nanoparticles and those of 7α-APTADD loaded nanoparticles.

3.3. Colloidal stability of nanoparticles

Both 7α-APTADD loaded nanoparticles and 7α-APTADD loaded Tf-nanoparticles precipitated during storage at 4 °C, but were easily re-dispersed upon gently shaking. No significant changes in particle size were observed for 1 week ($p > 0.05$) (Fig. 3) indicating that the nanoparticles were stable.

3.4. Expression of TfR on SKBR-3 and cellular uptake of nanoparticles

The result of the flow cytometry analysis of the TfR expression by SKBR-3 cells is shown in Fig. 4. It indicated that SKBR-3 cells expressed high level of TfR. The cellular uptake of calcein loaded

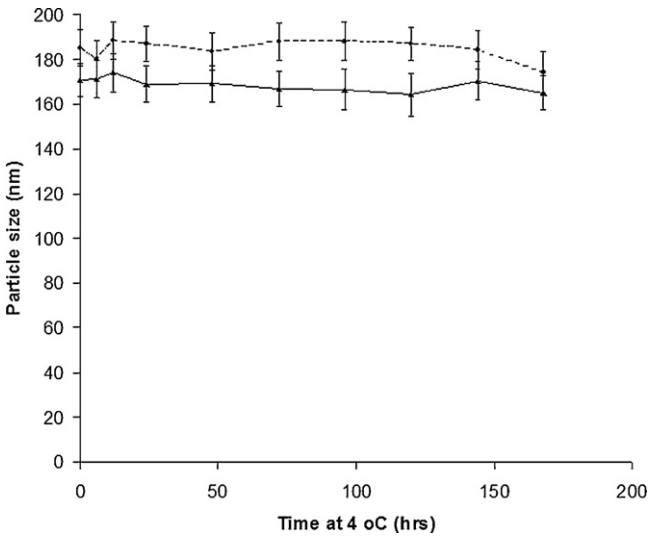

Fig. 3. Colloidal stability of the 7α-APTADD loaded nanoparticle (▲) and the 7α-APTADD Tf-loaded nanoparticle (●) during storage at 4 °C. The values in the plot were the means of three separate experiments. Error bars shown are the standard deviations.

nanoparticles was evaluated using flow cytometry. The cellular uptake of the Tf-nanoparticles was greatly enhanced relative to that of the non-targeted nanoparticles, suggesting that the efficient cellular uptake of the Tf-nanoparticles was a result of the Tf conjugation (Fig. 5A). Besides, the cellular uptake of the Tf-nanoparticles was blocked by addition of excess Tf in the media, which further demonstrated that the enhancement of Tf-nanoparticle cellular uptake was due to TfR (Fig. 5B).

The effect of the Tf-DOPE content on the cellular uptake of the Tf-nanoparticles was also examined. The mean fluorescence intensity (MFI) of cells treated by the Tf-nanoparticles with different mole% of Tf-DOPE is shown in Fig. 6. Cellular uptake of the Tf-nanoparticle with Tf-DOPE content of 0.6 mol% was higher than that of nanoparticles with Tf-DOPE content of 0.3 mol% ($p < 0.05$). However, further increase of the Tf-DOPE content resulted in decrease in the cellular uptake. Therefore, Tf-DOPE content of 0.6 mol% was used for further experiments.

Confocal laser scanning microscopy was used to examine the cellular uptake of the Tf-nanoparticles (Fig. 7). In the images of single cells, endosomal vehicles were clearly visualized in cells treated

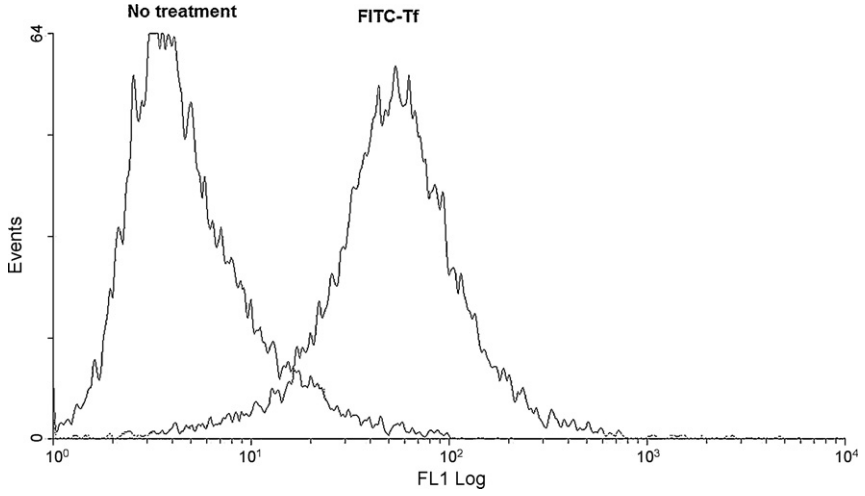

Fig. 4. Binding of FITC-Tf-to-TfR on SKBR-3 cells. Cells were incubated with FITC-Tf and cellular fluorescence was determined by flow cytometry. Results are shown in histogram with the *X*-axis indicating the cellular fluorescence intensity and the *Y*-axis indicating the cell count.

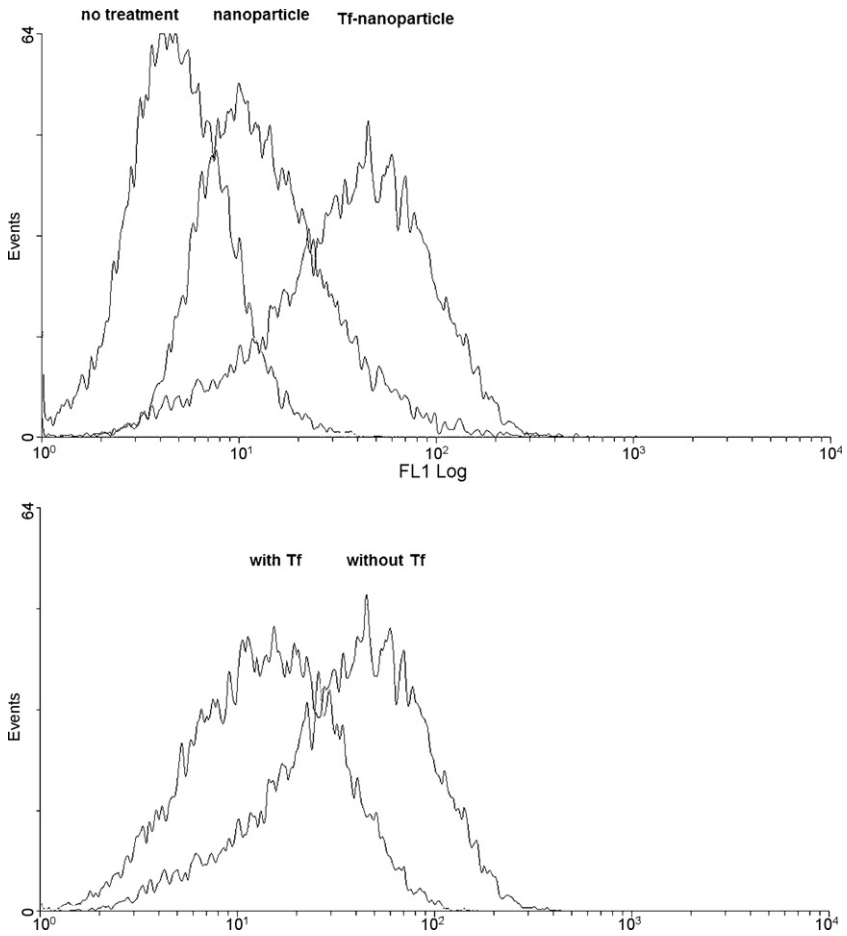

Fig. 5. Uptake of the nanoparticles by SKBR-3 cells. Cells were treated with calcein labeled nanoparticles and Tf-nanoparticles with a Tf-DOPE molar percentage of 0.6 mol%, and cellular fluorescence was measured by flow cytometry. Results are shown in histogram with the *X*-axis indicating the cellular fluorescence intensity and the *Y*-axis indicating the cell count. (A) Cells were treated with the nanoparticles and the Tf-nanoparticles and (B) cells treated with the Tf-nanoparticles were cultured in media with or without 20 μM Tf.

by Tf-nanoparticles indicating receptor-mediated endocytosis of the nanoparticles.

3.5. Cytotoxicity of the drug and the nanoparticles

Cytotoxicity of the free drug, the 7α-APTADD loaded Tf-nanoparticles and empty nanoparticles were evaluated. Following 24 h exposure, none of the agents caused significant cytotoxicity against SKBR-3 cells relative to DMSO, empty nanoparticles or water ($p > 0.05$) (Fig. 8). In addition, cells treated with DMSO, empty nanoparticles and water exhibited similar viability relative to cells without any treatment ($p > 0.05$, data not shown). In summary, both the drug and the nanoparticles were essentially non-toxic to SKBR-3 cells.

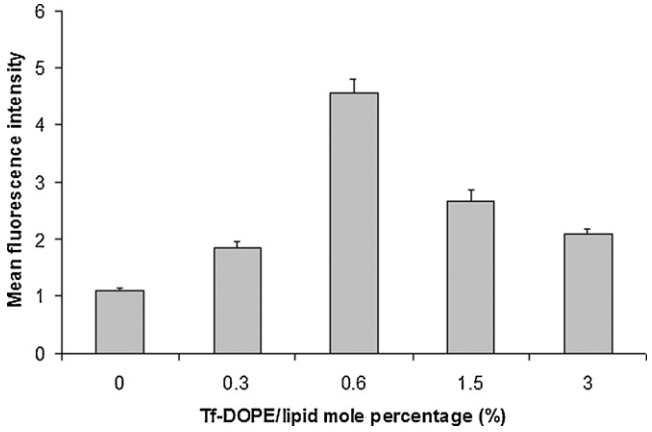

Fig. 6. MFI of cells treated by the Tf-nanoparticles with different molar percentages of Tf-DOPE.

3.6. Inhibition of SKBR-3 aromatase activity

Biological activities of 7α-APTADD free drug and 7α-APTADD loaded nanoparticles were evaluated in SKBR-3. The dose–response curves are shown in Fig. 9. Based on 3 separate experiments, the IC_{50} of 7α-APTADD free drug was in the range of 0.37–0.59 nM; the IC_{50} of the 7α-APTADD loaded nanoparticles was in the range of 1.90–3.41 nM and the IC_{50} of the 7α-APTADD loaded Tf-nanoparticles was in the range of 0.77–1.21 nM. The IC_{50} value of the free drug was found to be lower than the IC_{50} values of both the 7α-APTADD loaded nanoparticles and the 7α-APTADD loaded Tf-nanoparticles ($p < 0.05$). The observed increase in IC_{50} value due to nanoparticle encapsulation was consistent with attenuated drug release from the carrier (Song et al., 2009). Although this points to reduced bioactivity *in vitro*, the *in vivo* activity of the nanoparticles may nonetheless be greater due to anticipated increase in systemic circulation time and area under the plasma concentration versus time curve (AUC) for nanoparticles (Lu et al., 2007). In addition, we expect the nanoparticles synthesized in this study to have higher accumulation in tumor sites than free drug after adminis-

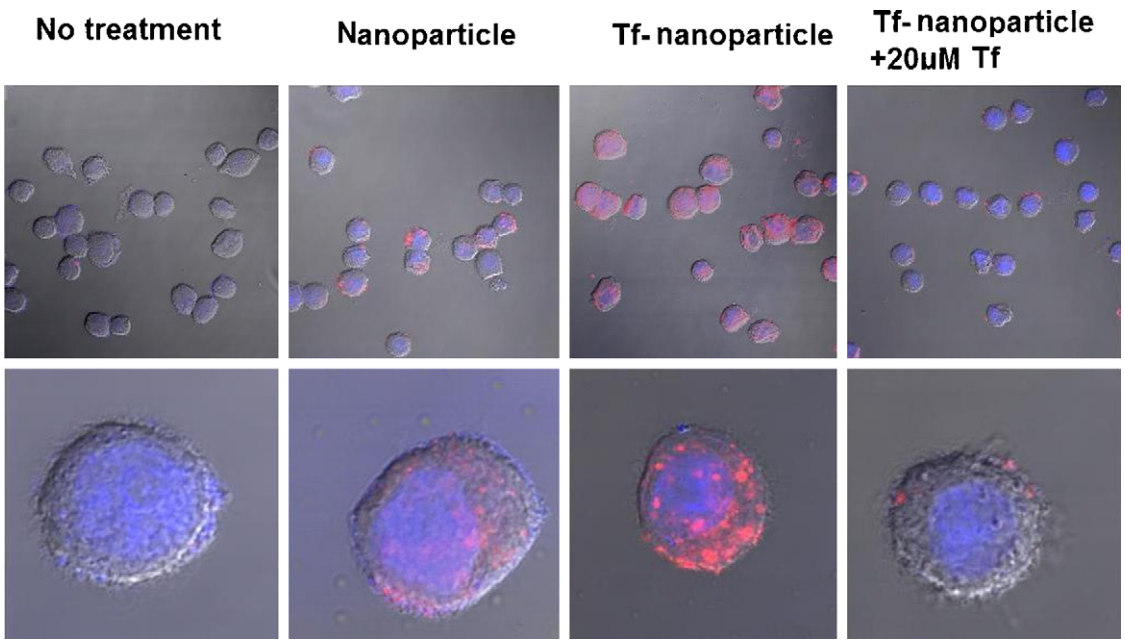

Fig. 7. Uptake of R18 labeled nanoparticle and Tf-nanoparticle in SKBR-3 cells. Cells were cultured in media with or without 20 μM Tf and visualized on a Zeiss LSM 510 META laser scanning confocal microscope.

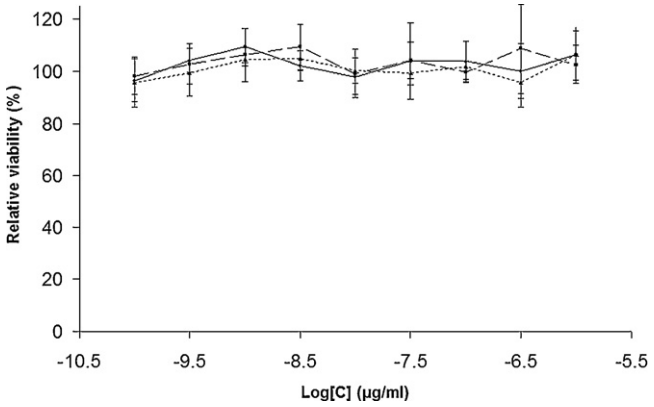

Fig. 8. Relative viability of cells treated by 7α-APTADD/DMSO solution (■), 7α-APTADD loaded Tf-nanoparticles (●) and empty nanoparticles (▲). The controls of the three samples were DMSO, empty nanoparticles and water, respectively.

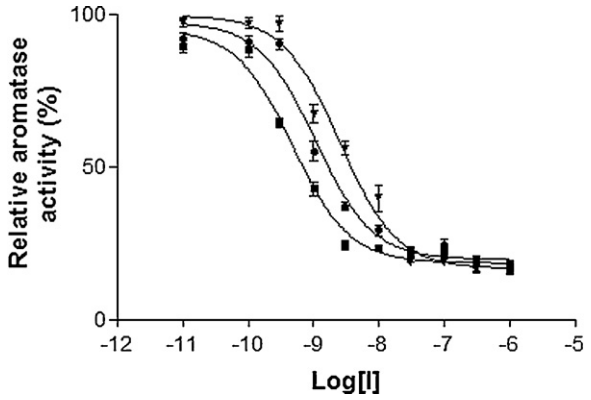

Fig. 9. Inhibition of aromatase activity in SKBR-3 cells cultures. Cells were treated with 7α-APTADD (■), the nanoparticles (▼) and the Tf-nanoparticles (●) at concentrations from 10 pM to 1 μM. The value for 100% estradiol formation in control cultures (no inhibitor) was 10.6 ± 3.3 pmol/ng DNA/h. Each point represents the average of nine determinations and the error bar shown was the standard error.

tration *in vivo* because of the enhanced permeability and retention (EPR) effect, which is known to affect nanoparticles (Bartlett et al., 2007). IC_{50} value of the non-targeted nanoparticles was significantly higher than that of the Tf-nanoparticle ($p < 0.05$). This might be due to the fact that the cellular uptake level of the Tf-nanoparticle was higher than that of the non-targeted nanoparticle due to the TfR-mediated endocytosis, which resulted in more accumulation of drug inside of cells.

4. Conclusions

TfR-targeted lipid-coated PLGA nanoparticles loaded with 7α-APTADD was synthesized and evaluated for aromatase inhibition efficiency. By optimizing the composition and synthesis protocol of the nanoparticles, the loading efficiency of the drug was maximized. Aromatase inhibition in breast cancer cells by the drug loaded Tf-nanoparticles was more effective than that by the non-targeted nanoparticles and was blocked by excess Tf in the media. The Tf-lipid-coated PLGA nanoparticles are promising vehicles for targeted delivery 7α-APTADD to breast cancer cells and warrant further investigation.

Acknowledgements

This work was supported in part by DOD grant W81XWH-08-1-0610 to Robert J. Lee, grant W81XWH-08-1-0521 to Robert W. Brueggemeier, NSF grant EEC-0425626 to L. James Lee and the State Scholarship Fund of the Ministry of Education of the P.R. China. "The project described was supported by Award Number UL1RR025755 from the National Center For Research Resources. The content is solely the responsibility of the authors and does not necessarily represent the official views of the National Center For Research Resources or the National Institutes of Health."

References

Ali, S.A., Joao, H.C., Hammerschmid, F., Eder, J., Steinkasserer, A., 1999. An antigenic HIV-1 peptide sequence engineered into the surface structure of transferrin does not elicit an antibody response. FEBS Lett. 459, 230–232.

Bartlett, D.W., Su, H., Hildebrandt, I.J., Weber, W.A., Davis, M.E., 2007. Impact of tumor-specific targeting on the biodistribution and efficacy of siRNA nanoparticles measured by multimodality *in vivo* imaging. Proc. Natl Acad. Sci. U.S.A. 104, 15549–15554.

Bershteyn, A., Chaparro, J., Yau, R., Kim, M., Reinherz, E., Moita, L.M., Irvine, D.J., 2008. Polymer-supported lipid shells, onions, and flowers. Soft Matter 4, 1787–1791.

Brueggemeier, R.W., Katlic, N.E., 1990. Aromatase inhibition by an enzyme-activated irreversible inhibiton in human carcinoma cell cultures. Cancer Res. 50, 3652–3656.

Brueggemeier, R.W., Reilly, J.M., Lovely, C.J., Ward, P.J., Quinn, A.L., Baker, D., Darby, M.V., Gu, X.J., Gilber, N.E., 1997. Biochemistry and pharmacology of 7α-substituted androstenediones as aromatase inhibitors. J. Steoid Biochem. Mol. Biol. 61, 247–254.

Brueggemeier, R.W., Hackett, J.C., Diaz-Cruz, E.S., 2005. Aromatase inhibitors in the treatment of breast cancer. Endocrinol. Rev. 26, 331–345.

Budhian, A., Siegel, S.J., Winey, K.I., 2007. Haloperidol-loaded PLGA nanoparticles: systematic study of particle size and drug content. Int. J. Pharm. 336, 367–375.

Bulun, S.E., Price, T.M., Aitken, J., Mahendroo, M.S., Simpson, E.R., 1993. A link between breast cancer and local estrogen biosynthesis suggested by quantification of breast adipose tissue aromatase cytochrome P450 transcripts using competitive polymerase chain reaction after reverse transcription. J. Clin. Endocrinol. Metab. 77, 1622–1628.

Chan, J.M., Zhang, L., Yuet, K.P., Liao, G., Rhee, J.W., Langer, R., Farokhzad, O.C., 2009. PLGA–lecithin–PEG core–shell nanoparticles for controlled drug delivery. Biomaterials 30, 1627–1634.

Chiu, S.J., Liu, S.J., Perrotti, D., Marcucci, G., Lee, R.J., 2006. Efficient delivery of a Bcl-2-specific antisense oligodeoxyribonucleotide (G3139) via transferrin receptor-targeted liposomes. J. Control Release 112, 199–207.

Duncanson, W.J., Figa, M.A., Hallock, K., Zalipsky, S., Hamilton, J.A., Wong, J.Y., 2007. Targeted binding of PLA microparticles with lipid-PEG-tethered ligands. Biomaterials 28, 4991–4999.

Eavarone, D.A., Yu, X., Bellamkonda, R.V., 2000. Targeted drug delivery to C6 gloma by transferrin-coupled liposomes. J. Biomed. Mater. Res. 51, 10–14.

Faulk, W.P., Hsi, B.L., Stevens, P.J., 1980. Transferrin and transferrin receptor in carcinoma of the breast. Lancet 2, 390–392.

Iinuma, H., Maruyama, K., Okinaga, K., Sasaki, K., Sekine, T., Ishida, O., Ogiwara, N., Johkura, K., Yonemura, Y., 2002. Intracellular targeting therapy of cisplatin encapsulated transferrin–polyethylene glycol liposome on peritoneal dissemination of gastric cancer. Int. J. Cancer 99, 130–137.

Inoue, T., Cavanaugh, P.G., Steck, P.A., Brv̈nner, N., Nicolson, G.L., 1993. Differences in transferrin response and numbers of transferrin receptors in rat and human mammary carcinoma lines of different metastatic potentials. J. Cell Physiol. 156, 212–217.

Jain, R.A., 2000. The manufacturing techniques of various drug loaded biodegradable poly(lactide-co-glycolide) (PLGA) devices. Biomaterials 21, 2475–2490.

James, V.H., Mcneill, J.M., Lai, L.C., Newton, C.J., Ghilchik, M.W., Reed, M.J., 1987. Aromatase activity in normal breast and breast tumor tissues: in vivo and in vitro studies. Steroids 50, 269–279.

Lu, Y.H., Wu, J., Wu, J.M., Gonit, M., Yang, X.J., Lee, A., Xiang, G.Y., Li, H., Liu, S.J., Marcucci, G., Ratnam, M., Lee, R.J., 2007. Role of formulation composition in folate receptor-targeted liposomal doxorubicin delivery to acute myelogenous leukemia cells. Mol. Pharm. 4, 707–712.

Miller, W.R., Mullen, P., Sourdaine, P., Watson, C., Dixon, J.M., Telford, J., 1997. Regulation of aromatase activity within the breast. J. Steroid Biochem. Mol. Biol. 61, 193–202.

Minko, T., 2006. Drug delivery system. In: Sinko, P.J. (Ed.), Martin's Physical Pharmacy and Pharmaceutical Sciences. Lippincott Williams & Wilkins, Philadelphia PA, p. 667.

Novozymes, 2007. Pharmaceut. Technol. Eur. 19, 10.

Rago, R., Mitchen, J., Wilding, G., 1990. DNA fluorometric assay in 96-well tissue culture plates using Hoechst 33258 after cell lysis by freezing in distilled water. Anal. Biochem. 191, 31–34.

Reed, M.J., Owen, A.M., Lai, L.C., Coldham, N.G., Ghilchik, M.W., Shaikh, N.A., James, V.H., 1989. *In situ* oestrone synthesis in normal breast and breast tumour tissues: effect of treatment with 4-hydroxyandrostenedione. Int. J. Cancer 44, 233–237.

Rossiello, R., Carriero, M.V., Giordano, G.G., 1984. Distribution of ferritin, transferrin and lactoferrin in breast carcinoma tissue. J. Clin. Pathol. 37, 51–55.

Savellano, D.H., Bos, E., Blondet, C., Sato, F., Abe, T., Josephson, L., Wissleder, R., Gaudet, J., Sgroi, D., Peters, P.J., Basilion, J.P., 2003. The transferrin receptor: a potential molecular imaging marker for human cancer. Neoplasia 5, 495–506.

Shindelman, J.E., Ortmeyer, A.E., Aussman, H.H., 1981. Demonstration of the transferrin receptor in human breast cancer tissue. Potential marker for identifying dividing cells. Int. J. Cancer 27, 329–334.

Snider, C.E., Brueggemeier, R.W., 1987. Potent enzyme-activated inhibition of aromatase by a 7α-substituted C19 steroid. J. Biol. Chem. 262, 8685–8689.

Song, X.R., Cai, Z., Zheng, Y., He, G., Cui, F.Y., Gong, D.Q., Hou, S.X., Xiong, S.J., Lei, X.J., Wei, Y.Q., 2009. Reversion of multidrug resistance by co-encapsulation of vincristine and verapamil in PLGA nanoparticles. Eur. J. Pharm. Sci. 37, 300–305.

Stano, P., Bufali, S., Pisano, C., Bucci, F., Barbarino, M., Santaniello, M., Carminati, P., Luisi, P.L., 2004. Novel camptothecin analogue (gimatecan)-containing liposomes prepared by the ethanol injection method. J. Liposome Res. 14, 87–109.

Yang, X., Koh, C.G., Liu, S., Pan, X., Santhanam, R., Yu, B., Peng, Y., Pang, J., Golan, S., Talmon, S., Jin, Y., Muthusamy, N., Byrd, J.C., Chan, K.K., Lee, L.J., Marcucci, G., Lee, R.J., 2009. Transferrin receptor-targeted lipid nanoparticles for delivery of an antisense oligodeoxyribonucleotide against Bcl-2. Mol. Pharm. 6, 221–230.